



## PAPER

## Self-subdiffusion in solutions of star-shaped crowders: non-monotonic effects of inter-particle interactions

## OPEN ACCESS

## RECEIVED

26 May 2015

## REVISED

7 October 2015

## ACCEPTED FOR PUBLICATION

9 October 2015

## PUBLISHED

9 November 2015

Content from this work  
may be used under the  
terms of the [Creative  
Commons Attribution 3.0  
licence](#).

Any further distribution of  
this work must maintain  
attribution to the  
author(s) and the title of  
the work, journal citation  
and DOI.

Jaehoh Shin<sup>1,2,4</sup>, Andrey G Cherstvy<sup>1</sup> and Ralf Metzler<sup>1,3</sup><sup>1</sup> Institute for Physics & Astronomy, University of Potsdam, 14476 Potsdam-Golm, Germany<sup>2</sup> Max Planck Institute for the Physics of Complex Systems, 01187 Dresden, Germany<sup>3</sup> Department of Physics, Tampere University of Technology, 33101 Tampere, Finland<sup>4</sup> Author to whom any correspondence should be addressed.E-mail: [jshin@pks.mpg.de](mailto:jshin@pks.mpg.de) and [rmetzler@uni-potsdam.de](mailto:rmetzler@uni-potsdam.de)**Keywords:** anomalous diffusion, crowded fluids, stochastic processesSupplementary material for this article is available [online](#)**Abstract**

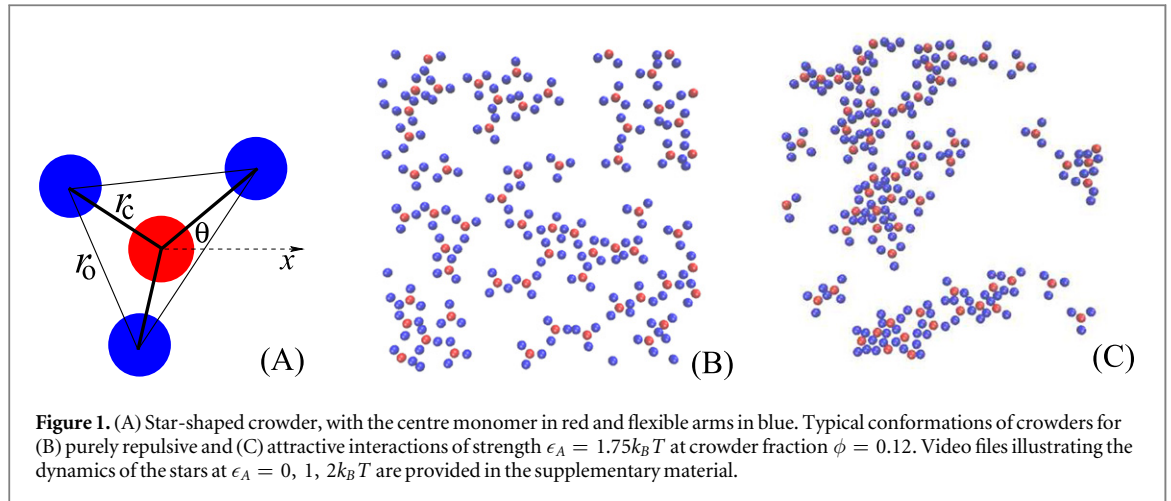
We examine by extensive computer simulations the self-diffusion of anisotropic star-like particles in crowded two-dimensional solutions. We investigate the implications of the area coverage fraction  $\phi$  of the crowders and the crowder–crowder adhesion properties on the regime of transient anomalous diffusion. We systematically compute the mean squared displacement (MSD) of the particles, their time averaged MSD, and the effective diffusion coefficient. The diffusion is ergodic in the limit of long traces, such that the mean time averaged MSD converges towards the ensemble averaged MSD, and features a small residual amplitude spread of the time averaged MSD from individual trajectories. At intermediate time scales, we quantify the anomalous diffusion in the system. Also, we show that the translational—but not rotational—diffusivity of the particles  $D$  is a nonmonotonic function of the attraction strength between them. Both diffusion coefficients decrease as the power law  $D(\phi) \sim (1 - \phi/\phi^*)^{2 \dots 2.4}$  with the area fraction  $\phi$  occupied by the crowders and the critical value  $\phi^*$ . Our results might be applicable to rationalising the experimental observations of non-Brownian diffusion for a number of standard macromolecular crowders used *in vitro* to mimic the cytoplasmic conditions of living cells.

**1. Introduction**

Over recent years, deviations from the standard Brownian diffusion law [1] have been observed in a broad range of systems, see the review articles [2–8]. Depending on the physical system under consideration, various theoretical models are used to describe these deviations [2–8]. Such *anomalous diffusion* is typically characterised by the power-law growth of the mean squared displacement (MSD) of particles with time

$$\langle \mathbf{r}^2(t) \rangle \simeq K_\beta t^\beta. \quad (1)$$

We distinguish subdiffusion for  $0 < \beta < 1$  and superdiffusion for  $1 < \beta$ . Subdiffusion is an abundant phenomenon for passive motion in the world of live biological cells [4–8]. In the biological context, subdiffusion was observed for particles ranging from small proteins [9, 10] via messenger RNA molecules [11] in the cell cytoplasm, to large chromosomal loci and telomeres in the nucleus [12], to submicron virus particles [13] and lipid granules [14]. The features of anomalous diffusion depend on the energy landscape and the physicochemical interactions in the system of particles [15, 16]. The advances of modern single particle tracking experiments [11, 17–21] provide a wealth of high resolution experimental data to quantitatively compare the microscopic mechanisms of non-Brownian diffusion with known theoretical models. The latter include, *inter alia*, the continuous time random walk [22–26] or the equivalent formulation in terms of fractional diffusion equations [3, 27], fractional Brownian motion [28], heterogeneous diffusion processes [29], scaled Brownian motion [30–33], as well as the fractional Langevin equation related to a viscoelastic environment [34, 35]. One



additional important type of anomalous diffusion models is the obstruction-mediated subdiffusion close to the percolation transition, see, e.g., [36–41].

The cytoplasm of biological cells is a superdense [11] fluid consisting of proteins, nucleic acids, membranous structures, cellular machinery components, semiflexible filaments, etc [42–45]. This macromolecular crowding reaches volume occupancies of  $\phi \gtrsim 30\%$  [46], not only affecting the rates of biochemical reactions and the kinetics of assembly processes in cells, but also believed to be contributing to the emergence of life [47]. In addition, the cytoskeletal meshwork [48] of eukaryotic cells impedes the diffusion of larger entities in cells, in particular, near the plasma membrane. The cytoplasm, in addition, is highly heterogeneous both in prokaryotic and eukaryotic cells [49–51]. The anomalous diffusion of cell-related phenomena may represent a blend of more than one theoretical model addressing the diffusion on different length and timescales [4, 5, 7, 52–57].

A number of experimental [58, 49], theoretical [59, 60], and simulation [46, 61–71] studies in recent years were devoted to tackling various aspects of particle diffusion in crowded environments. From the simulation perspective, for instance, studies of tracer diffusion in non-inert [72], heterogeneously distributed and polydisperse [73], restrictively mobile [61] squishy [59], and anisotropic [74, 75] obstacles were performed. The list of crowded three- and two-dimensional systems includes dense glassy systems of colloidal particles and hard spheres [76–78]. For instance, for hard disks diffusing in two dimensions, a series of substantial results are available from theoretical [82, 83], simulation [84, 85], and experimental [83, 86] studies. The dynamical glass transition [76–78] was investigated for amorphous and granular materials [79, 86] as well as for supercooled liquids [80], including some two-dimensional systems of soft discs [81]. The results for star-like crowders we present below can also be applied to dendronised polymers [87, 88], including charged dendrimers [89–91]. The dynamical and conformational properties of multi-arm polymers in free solutions [92, 93] and under confined conditions [94], is another possible application. Moreover, a number of single particle tracking, fluorescence correlation spectroscopy, and computer simulation studies of protein and lipid diffusion on crowded cell membranes indicated [95–100] the non-trivial effects of the particle shape. Indeed, our system of star-like crowders is expected to undergo a sort of glass transition at higher densities and stronger attractions, see below.

Despite the progress of analytical theories of crowded solutions, some important diffusive characteristics can only be studied quantitatively by computer simulations. This is particularly true for crowders of a non-trivial shape, such as star-like particles considered in the current paper (figure 1). We here use computer simulations to unravel the implications of the particle shape and ‘squishiness’ as well as the crowding fraction on the translational ( $D$ ) and rotational ( $D_r$ ) particle diffusivities in highly crowded solutions.

Our main target is to gain insight into the physical behaviour of nonspherical crowders *in vitro*. For the latter, soft non-spherical and often non-inert crowders such as globular PEG and branched dextran polymers are routinely used to mimic the effects of MMC in living cells. Another important experimental example is the diffusivity of anisotropic lysozyme-like proteins studied by Brownian dynamics simulations in crowded media [101]. It was demonstrated that—particularly in heavily crowded solutions—not only does a transient subdiffusion of the protein centre of mass exist, but also diffusion becomes progressively anisotropic. This anisotropy of the translational diffusion, pronounced on short-to-intermediate time scales, disappears on long time scales. The long time diffusivity values were shown to drop drastically with the protein concentration [101]. Moreover, the reduction of  $D_r$  for Y-shaped proteins such as IgG  $\gamma$ -Globulin (molecular weight of MW  $\approx 155$  kDa) was shown to be stronger than for more spherical proteins such as bovine serum albumin (MW  $\approx 66$  kDa). These experimental observations, based on fluorescence correlation spectroscopy measurements, are supported by all-atom Brownian dynamics simulations [101]. The inclusion of hydrodynamic interactions

revealed an additional reduction of  $D_r$  of proteins [102]. The reader is also referred to the simulation study [103] in which the self-diffusion of star-like polymers in the presence of hydrodynamic interactions [104] was examined in detail.

The paper is organised as follows. In section 2, we introduce our simulation model, the physical observables we are interested in, and some details on the data analysis algorithms. We present the main findings of our simulations in section 3. In section 4 the implications of our results for some cellular crowded systems are discussed.

## 2. Simulation model and observables

We implement our computer code, developed to simulate the particle diffusion of crowded solutions in which all particles are *explicitly* treated [66–68]. Here, we consider a two-dimensional system of star-shaped crowders, each consisting of four discs of diameter  $\sigma$  connected by elastic springs, see figure 1(A). The elastic potential between the midpoint of the molecule and the centres of the outer monomers is

$$U_c(r) = \frac{1}{2}k_s(r - r_c)^2, \quad (2)$$

where  $r_c$  is the equilibrium distance and  $k_s$  the spring constant. We also connect the outer monomers with springs of the same force constant  $k_s$ , namely

$$U_o(r) = \frac{1}{2}k_s(r - r_o)^2, \quad (3)$$

to mimic the softness of our triangular star-like crowders. The equilibrium distances and constants are set to  $r_c = 1.5\sigma$ ,  $r_o = 1.5\sqrt{3}\sigma$ , and  $k_s = 100k_B T/\sigma^2$ . Hereafter we use the symbol  $T$  as temperature in combination with the Boltzmann constant, otherwise it denotes the length of the recorded particle trajectory, see below.

The interaction between all beads is described by the 6–12 Lennard-Jones potential

$$U_{LJ}(r, r_{\text{cut}}) = 4\epsilon \left[ -\left(\frac{\sigma}{r}\right)^6 + \left(\frac{\sigma}{r}\right)^{12} \right] \Theta(r_{\text{cut}} - r) + C(r_{\text{cut}}). \quad (4)$$

Here  $\Theta(x)$  is Heaviside step function and  $C(r_{\text{cut}})$  is a constant that sets  $U_{LJ}(r > r_{\text{cut}}) = 0$ . For a purely repulsive potential, the standard cutoff distance  $r_{\text{cut}} = 2^{1/6}\sigma$  is used with the potential strength of  $\epsilon = k_B T$ . For attractive interactions we set  $r_{\text{cut}} = 2\sigma$  with varying adhesion strength  $\epsilon = \epsilon_A$  between the monomers. This attraction acts between all the monomers of the stars.

We use periodic boundary conditions within a square box of area  $L^2$ , to avoid finite-size artifacts. The packing fraction of  $M$  crowders in the system is defined as

$$\phi = MA/L^2,$$

where  $A = 4\pi(\sigma/2)^2$  is the total area of the four monomers and  $M \sim 10^2$  is a typical number of stars used in our simulations. In most scenarios below, the system size is  $L = 40\sigma$  and the total simulated trace length is  $T \sim 4 \times 10^8$ , in units of the elementary time step  $\Delta t$ . The size of the periodic box  $L$  was considerably larger than the correlation length of two crowders in the system which is about  $10\sigma$ , as estimated from the decay length of the pair interaction potential presented in figure 5 below.

The dynamics of the two-dimensional position  $\mathbf{r}_i(t)$  of the  $i$ th monomer disk interacting with the other monomer discs is described by the Langevin equation

$$m \frac{d^2 \mathbf{r}_i(t)}{dt^2} = -\gamma \frac{d\mathbf{r}_i(t)}{dt} - \sum_j \nabla \left[ U_c(r_{ij}) + U_o(r_{ij}) + U_{LJ}(r_{ij}) \right] + \xi_i(t). \quad (5)$$

Here  $\xi(t)$  represents Gaussian white noise with zero mean  $\langle \xi(t) \rangle = 0$  and correlator  $\langle \xi(t) \times \xi(t') \rangle = 4\gamma k_B T \delta(t - t')$ , with independent noise components along each Cartesian coordinate. Here  $k_B$  is the Boltzmann constant,  $\gamma$  is the friction coefficient (set to unity in all simulations below), and  $T$  the absolute temperature. In the following, we use  $\sigma$  and  $k_B T$  as the basic units of length and energy, respectively. We simulate the system in the  $NVT$  ensemble with the Verlet velocity algorithm with elementary integration time step  $\Delta t = 0.005$  for the total time  $T$ . The physical time scale in these simulations is the standard combination [105]

$$\delta\tau = \sigma \sqrt{m/(k_B T)} \approx 1 \text{ ns},$$

if we set the monomer diameter to  $\sigma = 6$  nm and its mass to the average mass of cytoplasmic crowders, namely  $MW \approx 68$  kDa [64, 106]. The time and the lag time are presented in the plots below in units of the elementary time scale  $\delta\tau$ .

Initially, we fix the position of all star-shaped particles and run the simulation for a time  $T_{\text{eq}}$  much longer than the relaxation time of the crowders. After this equilibration time, assessed in the absence of inter-crowder

attraction, we start measuring the positions and degrees of rotation of stars. Typically, we have  $T_{\text{eq}} = 1.5 \times 10^4$  (in terms of the elementary time  $\delta\tau$ ); this time gets longer for higher  $\phi$  fractions or larger attraction strengths  $\epsilon_A$ . It is at least two orders of magnitude longer than the typical relaxation time of a crowder,  $T_{\text{cr}} = 20 \dots 200$ . The latter was estimated from the relation

$$T_{\text{cr}} = (R_{\text{cr}}/\sigma)^2/D,$$

where  $R_{\text{cr}}$  is the radius of the four-monomer star and  $D$  is its average diffusivity.

We track the positions of the centre monomers of all the crowder stars and their orientation with respect to the  $x$ -axis, denoted by the angle  $\theta_i$ . From the trajectory of the  $i$ th crowder we calculate the time averaged translational ( $\overline{\delta_i^2}$ ) and rotational ( $\overline{\delta_{r,i}^2}$ ) individual MSD traces as [7]

$$\begin{aligned} \overline{\delta_i^2}(\Delta, T) &= \frac{1}{T-\Delta} \int_0^{T-\Delta} \left\{ [x_i(t+\Delta) - x_i(t)]^2 + [y_i(t+\Delta) - y_i(t)]^2 \right\} dt \\ &= \overline{\delta_{i,x}^2} + \overline{\delta_{i,y}^2} \end{aligned} \quad (6)$$

and

$$\overline{\delta_{r,i}^2}(\Delta, T) = \frac{1}{T-\Delta} \int_0^{T-\Delta} [\theta_i(t+\Delta) - \theta_i(t)]^2 dt. \quad (7)$$

Here  $\Delta$  is the lag time along the trace. In addition to the individual time averaged MSDs  $\overline{\delta^2}(\Delta)$  we compute the corresponding averages over the set of  $N$  trajectories,

$$\langle \overline{\delta^2}(\Delta) \rangle = \frac{1}{N} \sum_{i=1}^N \overline{\delta_i^2}(\Delta), \quad (8)$$

as well as their amplitude spread around this mean value.

The diffusion is called *ergodic* if the ensemble and time averaged MSDs coincide in the limit  $\Delta/T \rightarrow 0$  and if the spread of  $\overline{\delta^2}$  around the mean approaches the delta function in this limit [7, 107–110]. A more accurate description of ergodicity can be achieved based on the so called ergodicity breaking parameter EB [7]. The latter is defined as the variance of the distribution of the dimensionless variable

$$\xi = \overline{\delta^2} / \langle \overline{\delta^2} \rangle,$$

namely [7]

$$\text{EB}(\Delta) = \langle \xi^2(\Delta) \rangle - \langle \xi(\Delta) \rangle^2 = \langle \xi^2(\Delta) \rangle - 1. \quad (9)$$

For the standard Brownian motion we have [110]

$$\text{EB}_{\text{BM}}(\Delta) = \frac{4}{3} \frac{\Delta}{T}. \quad (10)$$

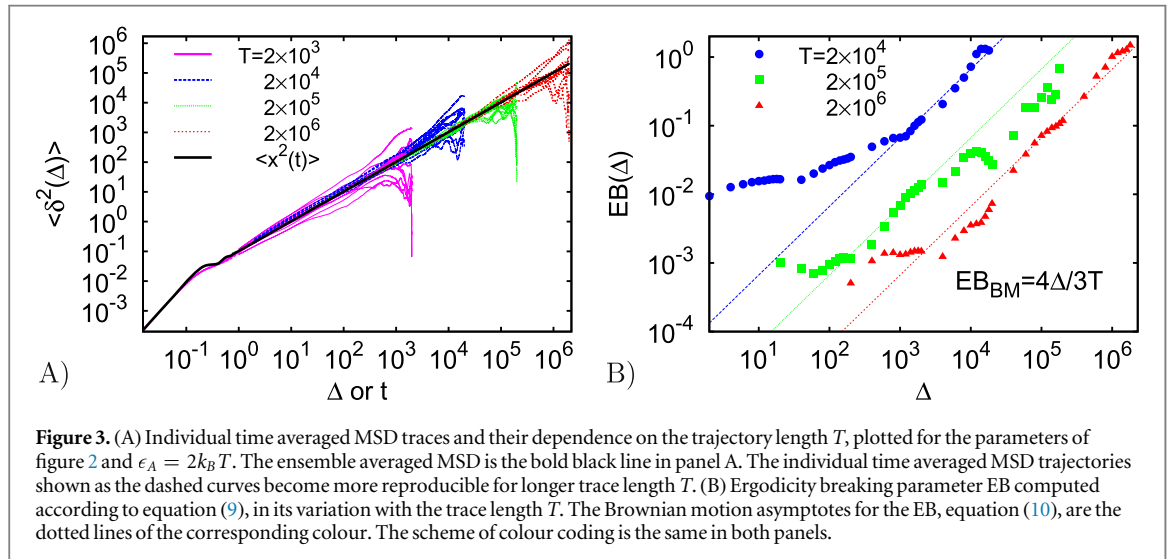
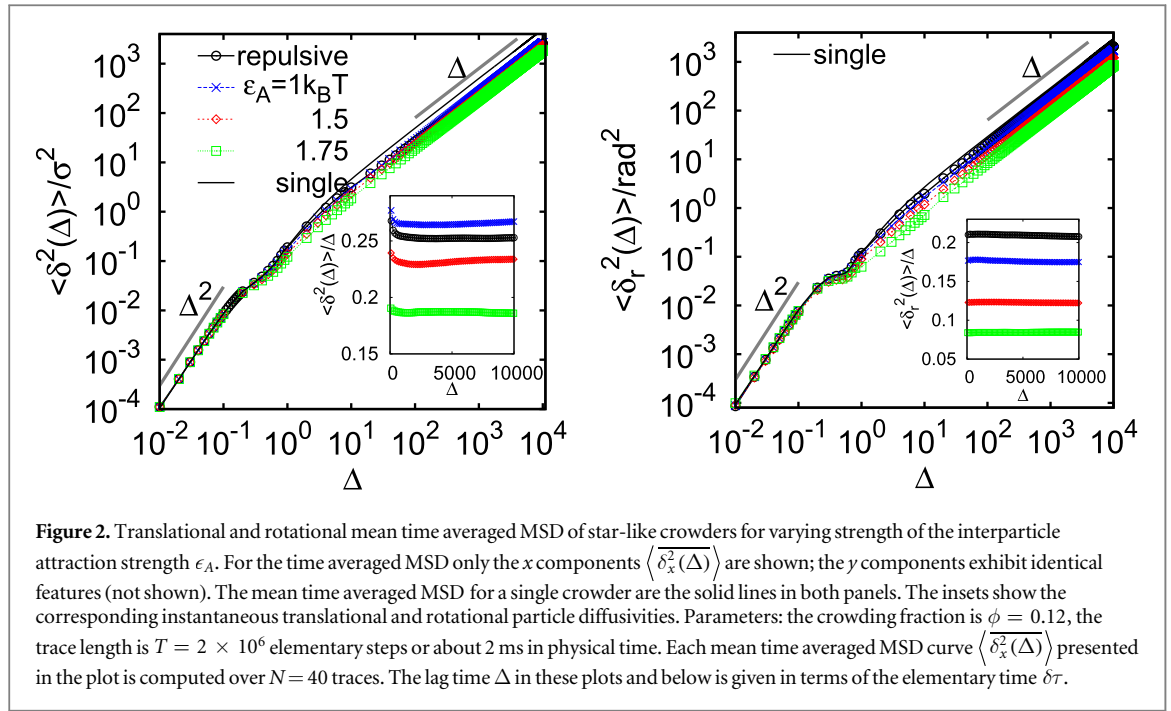
## 3. Results

### 3.1. Time averaged MSD and ergodicity breaking parameter

In figure 2, we present the behaviour of the translational and rotational MSDs for varying interparticle attraction strength  $\epsilon_A$  at crowder packing fraction  $\phi = 0.12$ . The initial crowder diffusion is ballistic, stemming from the simulation of inertial particles, see also [18, 72, 79, 82, 86] for other simulations and experimental results. At intermediate time scales of  $\Delta \sim 0.1 \dots 10$  we observe a nonmonotonic behaviour of the time averaged MSD that we ascribe to the events of the first collision of a given crowder molecule with another crowder and the oscillations of the centre monomers connected by its springs. In the long lag time limit the translational and rotational MSDs grow linearly with  $\Delta$  reflecting the Brownian behaviour of the crowder particles.

The region of non-Brownian diffusion is centred at  $\Delta \sim 1$  or at about 1 ns in the physical time. Note that for larger tracers, as often used in single particle tracking experiments, the elementary time scale will increase correspondingly and the region of transient anomalous diffusion will shift to longer times. The time span of anomalous diffusion can be extended—as compared to the current self-diffusion in the sea of mobile crowders—if the obstacles/crowders are partly or fully immobilised, see the results of [61, 72].

In this limit the diffusion is ergodic, as we demonstrate in figure 3(A),B. This statement is not necessarily trivial: in many weakly non-ergodic systems the time averaged MSD turns out to be a linear function of the lag time  $\Delta$  while the ensemble averaged MSD scales as a power-law or logarithmically in time  $t$ . This phenomenon was observed in a number of experiments [14, 54–56] and explained in terms of various stochastic processes [7, 29, 30, 111–119]. Figure 3(A) demonstrates both that to very good approximation ergodicity in the sense of



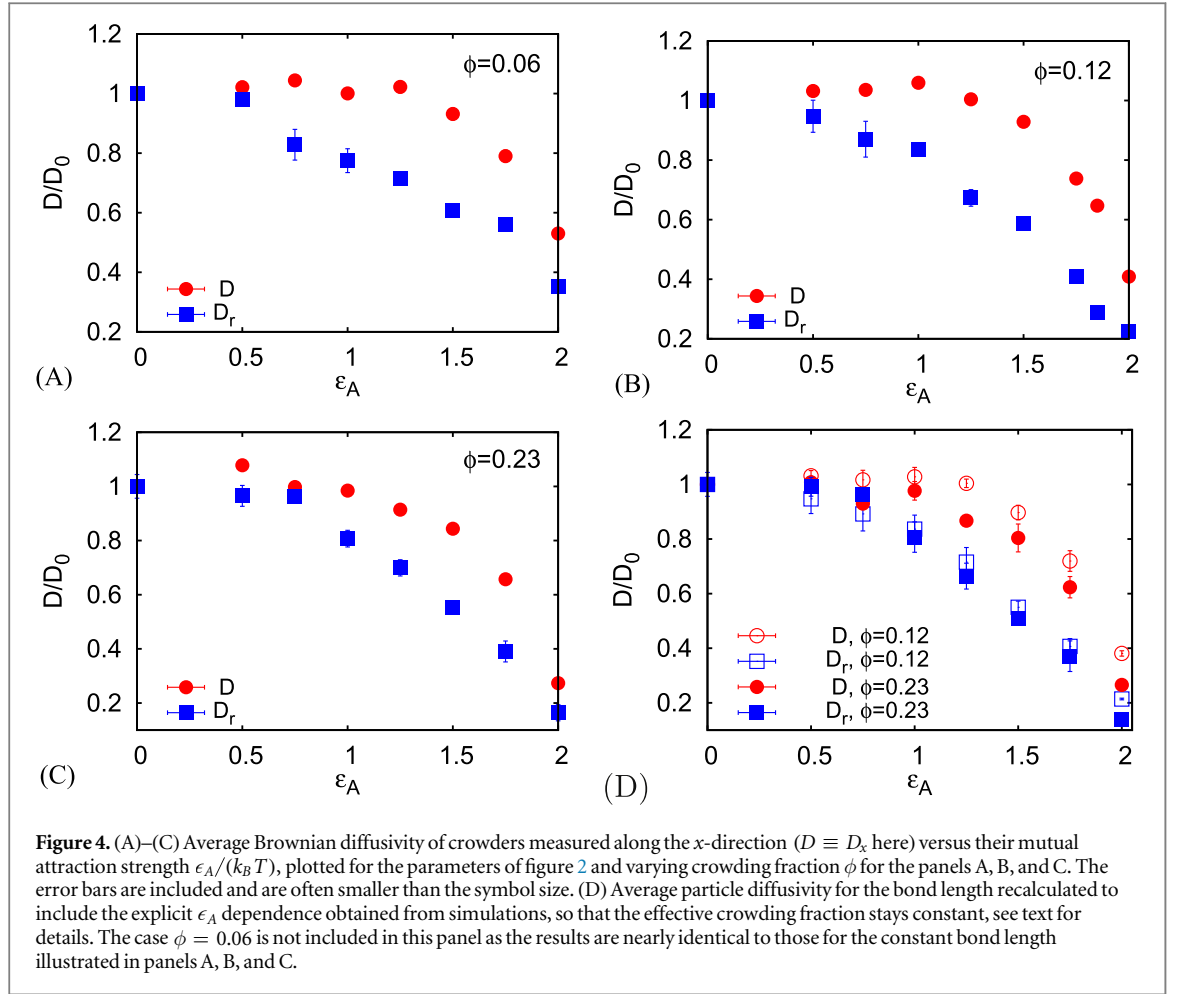
the equality

$$\langle x^2(\Delta) \rangle = \overline{\delta^2(\Delta)}$$

is fulfilled and that a very small amplitude scatter around the mean  $\langle \delta^2(\Delta) \rangle$  exists and thus the individual time averages are reproducible quantities. We furthermore detail the dependence of the particle diffusivity in this Brownian limit versus the attraction strength and the filling fraction in figures 4 and 7, respectively.

Let us be more specific. Figure 3(A) illustrates the time averaged MSD for different lengths of the time series as well as the superimposed ensemble averaged MSD shown as the bold black line. As can be seen from the figure, the amplitude scatter of single traces  $\delta^2$  around their mean remains small along the entire trajectory, except when  $\Delta \sim T$ , as expected. This growing spread as  $\Delta \sim T$  is a standard feature of even canonical Brownian motion appearing due to progressively poorer statistics when taking the time average [7].

More importantly we observe that the amplitude spread of the time averaged MSD at a fixed lag time  $\Delta$  decreases as the length  $T$  of the time traces increases. This property is ubiquitous for ergodic diffusion processes [7]. We note that the magnitude of the amplitude scatter that we observe for  $\overline{\delta^2}$  for moderately adhering star-shaped crowders are similar to that of a tracer in a network of sticky spherical obstacles, compare figure 3(A) above and figure 7 in [72]. Computing the magnitude of the mean time averaged MSD for varying trace length  $T$



we observe that its magnitude stays nearly unchanged with  $T$  (figure 3(A)). In the short lag time regime the ballistic scaling is visible.

These observations as well as the explicit evaluation of the ergodicity breaking parameter EB in equation (10) indicate that even at moderate strengths of attraction the diffusion of our crowders stays ergodic. Namely, in figure 3(B) we demonstrate that—using the individual time averaged MSD traces from simulations—the ergodicity breaking parameter (9) follows at intermediate-to-long times the theoretical asymptote for the Brownian motion, equation (10). The EB grows linearly with the lag time  $\Delta$  and decreases with the length of the trajectory as  $EB(T) \sim 1/T$ , see figure 3(B). Some discrepancies from the theoretical prediction (10) we observe at short times stem likely from the ballistic and anomalous diffusion regimes of the time averaged MSD traces at small  $\Delta$  values. Our process is thus fundamentally different from other anomalously diffusive systems such as those described by continuous time random walks [7] or heterogeneous diffusion processes [29]. For the latter a pronounced scatter of the time averaged MSD trajectories around their mean and a clear dependence of the amplitude of  $\langle \delta^2(\Delta) \rangle$  on  $T$  at fixed  $\Delta$  exist, that is, the system ages [7, 120, 121].

### 3.2. Crowder diffusivity and anomalous scaling exponent

The particle diffusivities are defined in our simulations as

$$D_x = \frac{\langle \delta_x^2(\Delta) \rangle}{2\Delta} \quad (11)$$

and

$$D_r = \frac{\langle \delta_r^2(\Delta) \rangle}{2\Delta} \quad (12)$$

obtained from the linear behaviour of the mean time averaged MSD in the long time limit  $\Delta \gg 1$ . Figure 4 shows the values of  $D$  and  $D_r$  extracted from a linear fit of the translational and rotational time averaged MSDs in

the range  $\Delta = 10^3 \dots 10^4$ . We find that while the rotational diffusivity  $D_r$  decreases monotonically, the translational diffusivity exhibits a shallow yet significant maximum at  $\epsilon_A^* \approx 1k_B T$ . This systematic trend persists for the variation of the crowder fraction in a quite broad range (figure 4). This implies that the self-diffusion of our star-like crowders can be facilitated by a weak interparticle attraction. This is one of the main conclusions of this study. One can rationalise this trend in the self-diffusion in terms of the concept of the *effective crowder size* that decreases for moderate attraction strengths  $\epsilon_A \approx 1k_B T$ .

Note that, as we work in the *NVT*-ensemble, the number of particles in the simulation box stays constant, whereas their effective size decreases with the strength of attraction  $\epsilon_A$  between the monomers. Upon increase of  $\epsilon_A$  the bond length of the stars decreases, namely about 0.8% for  $\epsilon_A = 1k_B T$  and 1.78% for  $\epsilon_A = 2k_B T$ . With this change of the bond length the effective crowding fraction gets smaller too for higher attraction strengths. If we account for this effect and keep the *crowding fraction constant* via adjusting the number of particles in the simulation box upon variations of  $\epsilon_A$ , the nonmonotonic behaviour of  $D(\epsilon_A)$  indeed becomes slightly weaker, as demonstrated in figure 4(D). The optimal attraction strength, however, remains of the order of the thermal energy.

Figure 4 illustrates that for progressively stronger star–star attraction their mutual diffusivity decreases eventually to zero due to aggregate formation, see also figure 5 and its discussion below. Also note that the reduction of the rotational diffusion coefficient starts at smaller crowding fractions, see the blue squares in figure 4, as compared to the translational motion that might also feature a nonmonotonic behaviour. The relative reduction of the rotational diffusivity by crowding is also comparatively stronger, as physically expected, because of geometric frustration and overlapping with radially quite inflexible/non-responsive crowders.

We also detect a progressive *aggregation of crowders* at relatively large crowder–crowder attraction strengths  $\epsilon_A$ , as demonstrated in figure 1(C) and in the video files in the supplementary material. This is a well-known phenomenon, for instance, in the glass transitions of dense suspensions of sticky hard spheres [122]. Accordingly, the average diffusivity  $D$  of crowders as plotted in figure 4 decreases due to the averaging over an ensemble of particles that perform individual random motions. This average takes into account both particles forming transient aggregates as well as free particles. Roughly speaking the average diffusivity drops inversely proportionally to the number of particles in the *cluster*. The fraction of particles clustering in these aggregates increases with the mutual attraction strength. The average diffusivity therefore progressively decreases with  $\epsilon_A$  due to a larger fraction of particles in transient aggregates.

At large attraction strength the majority of particles belong to big clusters (results not shown) which diffuse in a Brownian fashion as a whole, with the diffusivity correspondingly reduced by the cluster size. We observe that larger attraction strengths effectively reduce the temperature in the system of crowders, thus favouring aggregation. This temperature argument, however, gets reverted for the self-diffusion of weakly attractive stars, when at a fixed number of particles the crowders becomes slightly smaller and thus diffuse faster for stronger inter-particle attraction.

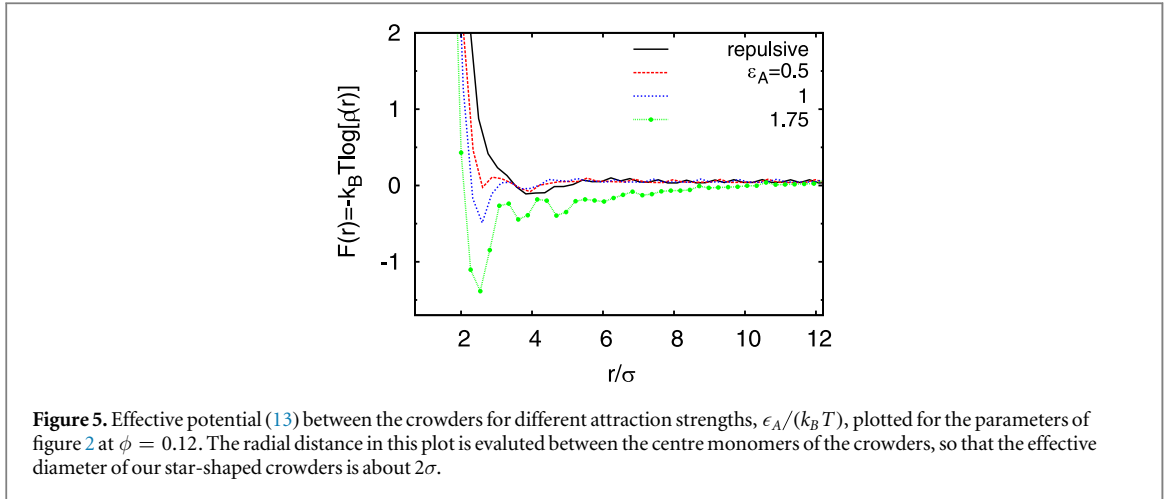
At a fixed cohesiveness  $\epsilon_A$  of our stars, vicinal crowders create a rough energy landscape for the self-diffusion and the hopping of a given crowder particle. As the MMC fraction  $\phi$  increases, the binding events give rise to a prolonged particle aggregation and reduced self-diffusivity. Above a critical MMC fraction, the barrier height exceeds the thermal energy, thus increasing the lifetime of crowder aggregates significantly. For stronger star–star attraction, the formation of essentially permanent aggregates sets in for less crowded systems, leading to an inhomogeneous, phase-separated spatial distribution, see figure 1(C).

A nonmonotonicity of the translational diffusivity  $D$  at similar strengths of the particle–crowder attraction was found in [64] for the tracer diffusion in dense suspensions of spherical Brownian particles. While we here detect that the attraction strength yielding the highest value of  $D$  is a function of the crowding fraction  $\phi$  of the stars for the spherical particles, the stickiness facilitating the particle diffusivity was almost  $\phi$ -independent in [64]. The nonmonotonic  $D(\epsilon_A)$  dependence was interpreted in [64] in terms of the roughness of the free-energy landscape for the tracer diffusion using the concept of the chemical potential. Interestingly, the tracer diffusivity was also nonmonotonic in  $\phi$  in a static regular array of sticky obstacles, as quantified in [72].

We checked the universality of the observed dependencies for  $D(\epsilon_A)$  and  $D(\phi)$  also for disk-like particles. Namely, we simulated just a single monomer of our star-shaped crowders with the given adhesive properties. The diffusivity was indeed found to reveal a maximum at  $\epsilon_A^{\text{opt}} \sim 0.5 \dots 1k_B T$  (not shown), indicating some universality of this *a priori*, counterintuitive, faster diffusion for a weak interparticle attraction [64]. Note also that for a polymer chain diffusing in an array of sticky obstacles, a weak chain–obstacle attraction can also substantially enhance the polymer diffusivity [64, 123].

To rationalise the observed behaviour of  $D(\epsilon_A)$ , we calculate in figure 5 the potential of the mean force between two crowders as

$$F(r) = -k_B T \log[\rho(r)]. \quad (13)$$



In this reconstructed, approximate free energy (valid for dilute systems only) the quantity  $\rho(r)$  is the average radial distribution function of the centre crowders monomer in the steady-state long time limit. As the mutual attraction strength  $\epsilon_A$  increases, we observe that the potential well at the separation  $r \approx 2\sigma$  becomes deeper, see the first well in figure 5. Concurrently, the distance at which  $F(r)$  sharply increases becomes shorter for larger  $\epsilon_A$ . For a stronger star–star attraction the crowders feature a more organised appearance, resulting in measurable oscillations of  $\rho(r)$  and  $F(r)$ , as evidenced in figure 5.

These trends indicate that the effective crowder radius gets smaller with increasing  $\epsilon_A$ , and, at an optimal value  $\epsilon_A^{\text{opt}}$ , the crowders approach one another more closely, yet without sticking. This in turn might result in a faster average diffusivity  $D$  at  $\epsilon_A \approx \epsilon_A^{\text{opt}}$ , as we indeed observe. An effective reduction of the crowder size at optimal attraction strength is one important cause—albeit possibly not the only one—for this facilitated diffusion. In the current system, the equilibrium distance of the outer monomers from the central monomer is reduced by about 2% for the inter-monomer attraction strength of  $2k_B T$ . Even higher values of  $\epsilon_A$  give rise to the formation of large clusters of crowders, see the supplementary material. As shown in figure 4, the corresponding diffusivity of an average particle drops dramatically with  $\epsilon_A$ .

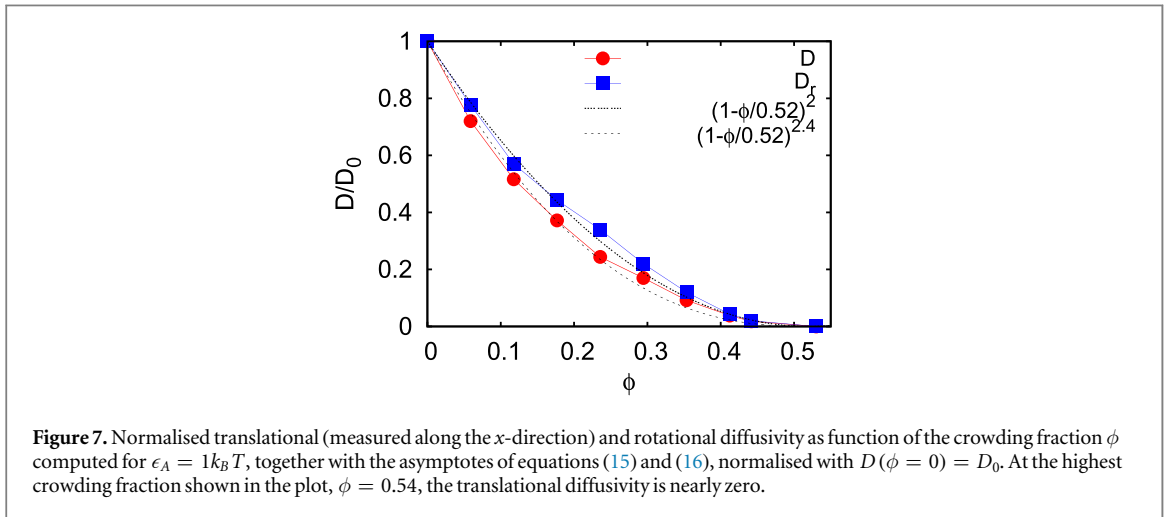
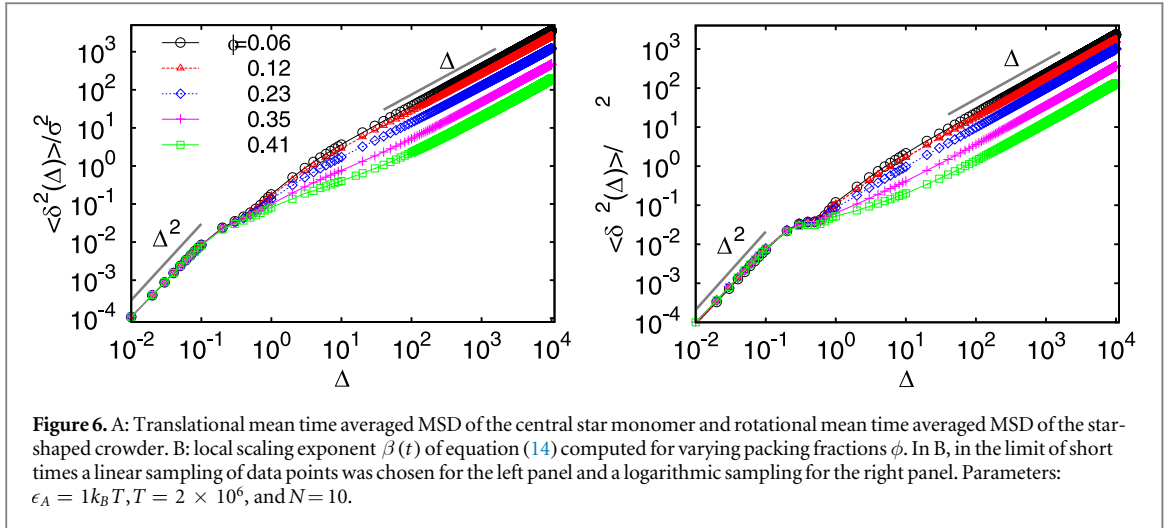
In figure 6(A), we show the translational and rotational MSD for varying packing fraction of crowders  $\phi$ . As expected—from a linear fit to the long time time averaged MSD—the diffusivity is a monotonically decreasing function of  $\phi$ , as evidenced by figure 7. For more severely crowded systems, the tracer diffusion gets more obstructed and the magnitude of the corresponding mean time averaged MSD  $\langle \delta^2 \rangle$  decreases. To elucidate these effects further, we evaluate from the time averaged MSD traces of figure 6(A) for the translational motion the local diffusion exponent [7, 124]

$$\beta(\Delta) = \frac{d \log \left( \langle \overline{\delta^2(\Delta)} \rangle \right)}{d \log(\Delta)}. \quad (14)$$

For the rotational motion the exponent  $\beta_r(t)$  is defined analogously.

We observe a ballistic regime with  $\beta \approx 2$  in the particle diffusion at short times, figure 6(B). This ballistic regime is followed by a decrease and further increase of the scaling exponent at  $\Delta \sim 1$ . These nonmonotonic trends are also clearly visible from the behaviour of the time averaged MSD traces themselves as a function of the lag time  $\Delta$ , see figure 6(A). We find that the variations of the scaling exponent for translational and rotational motions of the star-like crowders appear correlated, indicating a coupling of these diffusion modes [20]. In the plots for the scaling exponent  $\beta(t)$  in figure 6(B) the significant spike-like signal at  $\Delta \sim 1$  is interpreted as an effect of the first collision of particles and the resulting onset of an effective confinement. We note that even in effective one-particle theories pronounced oscillations occur at the crossover point between the initial ballistic and the overdamped regime [125, 126].

With increasing crowder fraction  $\phi$  we also observe a more pronounced range of anomalous diffusion for lag times of the order of  $\Delta \sim 1 \dots 100$ . This range appears strongly correlated for rotational and translational particle motion, as shown in figure 6(B). For rotational diffusion, the scaling exponent drops practically to zero for times longer than those of the initial ballistic growth, and the corresponding mean time averaged MSD trace  $\langle \delta_r^2 \rangle$  exhibits a short plateau (figure 6(B)). Such a transient subdiffusion was observed for a number of systems [5–7], see also the Introduction. Especially in dense colloidal systems close to the glass transition at  $\phi = \phi^*$  this subdiffusion is accompanied by an exponential growth of the solution viscosity  $\eta = \eta(\phi)$ , which is divergent at  $\phi \rightarrow \phi^*$  [76]. The colloidal glasses also exhibit progressive particle localisation effects as discussed in [76, 77]. In



the long lag time limit the exponent becomes Brownian  $\beta \approx 1$  for the crowded systems far from the critical occupation  $\phi^*$ .

Remarkably, the relative variation of the translational and rotational diffusivities with the crowding fraction of stars is quite similar. For comparison, we plot in figure 7 the theoretical prediction for dense suspensions of hard spheres [127, 128]

$$\frac{D(\phi)}{D(0)} = \left[ 1 - \frac{\phi}{\phi^*} \right]^2, \quad (15)$$

with the critical packing fraction for our system of  $\phi^*(\epsilon_A = 1k_B T) \sim 0.52$  that provides the best fit to the data. Above this value  $\phi^*$  both translational and rotational diffusivities of the crowders essentially *vanish*. If the explicit dependence of the particle size on the attraction strength is taken into account, as in Panel D of figure 4, the critical fraction  $\phi^*$  also becomes a function of  $\epsilon_A$ . At this critical crowding fraction the interparticle attraction becomes so strong that the self-diffusion is almost completely localised and the motion of particles corresponds more to a very restricted wiggling and jigging. The translational MSD of individual crowders—after subtracting the diffusive motion of the entire cluster as a whole—saturates to a plateau with the scaling exponent  $\beta \rightarrow 0$  (results not shown). As expected, when the star–star interactions become stronger, some aggregate formation sets in for less crowded systems, and thus the critical value  $\phi^*$  is diminished (not shown). Albeit the theory in [127, 128] is developed for three-dimensional suspensions in the presence of hydrodynamic interactions, it agrees remarkably well with our results, as shown in figure 7. The reader is also referred to [129] for experimental data of the crowding dependent diffusivity of colloidal particles and alternative theoretical predictions for the diffusivity  $D(\phi)$ .

We note that [130] suggest exponential rather than power-law forms for the particle diffusivity in crowded solutions. Also, different scalings with the crowding fraction were predicted for semi-dilute solutions of multi-arm polymers and hyper-stars [92], where  $D(\phi) \sim \phi^{-1/2}$ . The polymeric nature of star arms plays, however, a dominant role in this scaling relation. Also, the decrease of the particle diffusivity in a system of polydisperse hard disks exhibiting a glass transition was shown to follow the relation [82, 85]

$$D(\phi) \sim (\phi - \phi^*)^{2.4}, \quad (16)$$

in agreement with the results of the mode coupling theory, see, e.g., [83, 131]. In figure 7, we present both theoretical asymptotes with the scaling exponents of 2 and 2.4, equations (15) and (16). The latter indeed fits better the decrease of the translational diffusivity  $D(\phi)$  of star-like crowders, but not the rotational diffusivity  $D_r(\phi)$ . From the limited simulation data available we cannot determine the value of the scaling exponent more precisely.

## 4. Conclusions

We performed extensive computer simulations and theoretical data analysis of the diffusion of crowders with a branched structure. A simple example of such spiky but responsive crowders in two dimensions are deformable star-shaped crowders employed here. Their outer monomers are interconnected by an elastic potential, bestowing upon it a certain degree of responsiveness—an important characteristics for many polymeric crowders [59]. We also incorporated in the simulations an interparticle attraction strength which represents another realistic feature of solutions of non-ideal crowders *in vitro*.

We found that the diffusion of our star-like crowders is ergodic and, within accuracy, Brownian in the long time limit. We examined the behaviour of the ensemble averaged MSD and the time averaged MSDs of the crowders in a wide range of MMC fraction  $\phi$  and the inter-crowder attraction strength  $\epsilon_A$ . As a function of the crowding fraction, we demonstrated that both translational  $D$  and rotational  $D_r$  diffusivities approximately follow the analytical decrease (15) of  $D(\phi)$  predicted for suspensions of hard spheres. The dependence of the star–star attraction strength is more remarkable. Namely, the translational diffusivity shows a weak yet systematic nonmonotonic dependence on  $\epsilon_A$  for the solutions at all crowding fractions studied herein. The rotational diffusivity, in contrast, is a monotonically decreasing function of the interparticle attraction strength  $\epsilon_A$ . Thus, a relatively weak intermonomer attraction can facilitate the lateral diffusion and also induce a certain degree of clustering and spatial heterogeneities in crowded solutions of non-inert particles.

These effects will impact the diffusion of a tracer particle in crowded solutions—such as those of PEG, dextran, or Ficoll—used *in vitro* to mimic the crowded conditions in living cells [59, 62]. In addition to the proof of the ergodic long lag time diffusion shown in figure 3, and the transient subdiffusion regime of our star-like crowders in figure 6, the dependencies of the diffusivities are the principal results of the current study. Of course, our planar triangle-like stars still represent quite a primitive system to mimic the non-ideal shape of real crowders in experimentally relevant setups. Future investigations, including a three-dimensional pyramid-like shape of crowders with longer polymeric arms, will further elucidate the physical consequences of non-spherical and squishy crowders, and potentially exhibit additional unexpected behaviour. Moreover, not only is the self-diffusion to be studied but also the diffusion of tracer particles of various sizes and shapes in such crowded suspensions [70], as well as poly-disperse mixtures of crowders [70, 132], should be investigated. Some asymmetry may also be incorporated into the crowder shape. Recently, single-particle tracking measurements allowed one to rationalise the translational and rotational diffusivities of micron-size symmetric and asymmetric boomerang-shaped particles in two dimensions [133]. It was observed that the regimes of Brownian diffusion exist at short and long times while a coupling of  $D$  and  $D_r$  gave rise to subdiffusion at intermediate times.

## Acknowledgments

We acknowledge funding from the Academy of Finland (Suomen Akatemia, Finland Distinguished Professorship to RM), Deutsche Forschungsgemeinschaft (DFG Grant to AGC), and the Federal Ministry of Education and Research (BMBF Project to JS).

## References

- [1] Einstein A 1905 *Annal. Physik* **322** 549
- [2] Bouchaud J-Ph and Georges A 1990 *Phys. Rep.* **195** 127
- [3] Metzler R and Klafter J 2000 *Phys. Rep.* **339** 1
- [4] Barkai E, Garini Y and Metzler R 2012 *Phys. Today* **65** 29
- [5] Sokolov I M 2012 *Soft Matter* **8** 9043

- [6] Höfling F and Franosch T 2013 *Rep. Progr. Phys.* **76** 046602
- [7] Metzler R, Jeon J-H, Cherstvy A G and Barkai E 2014 *Phys. Chem. Chem. Phys.* **16** 24128
- [8] Meroz Y and Sokolov I M 2015 *Phys. Rep.* **573** 1
- [9] Banks D S and Fradin C 2005 *Biophys. J.* **89** 2960
- [10] Weiss M, Elsner M, Kartberg F and Nilsson T 2004 *Biophys. J.* **87** 3518
- [11] Golding I and Cox E C 2006 *Phys. Rev. Lett.* **96** 098102
- [12] Bronstein I, Israel Y, Kepten E, Mai S, Shav-Tal Y, Barkai E and Garini Y 2009 *Phys. Rev. Lett.* **103** 018102
- Burnecki K, Kepten E, Janczura J, Bronshtein I, Garini Y and Weron A 2012 *Biophys.* **103** 1839
- [13] Seisenberger G, Ried M U, Endress T, Büning H, Hallek M and Bräuchle C 2001 *Science* **294** 1929
- [14] Jeon J-H, Tejedor V, Burov S, Barkai E, Selhuber-Unkel C, Berg-Sorensen K, Oddershede L and Metzler R 2011 *Phys. Rev. Lett.* **106** 048103
- [15] Khoury M, Lacasta A M, Sancho J M and Lindenberg K 2011 *Phys. Rev. Lett.* **106** 090602
- [16] Skaug M J, Lacasta A M, Ramirez-Piscina L, Sancho J M, Lindenberg K and Schwartz D K 2014 *Soft Matter* **10** 753
- [17] Kusumi A, Nakada C, Ritchie K, Murase K, Suzuki K, Murakoshi H, Kasai R S, Kondo J and Fujiwara T 2005 *Annu. Rev. Biophys. Biomol. Struct.* **34** 351
- [18] Huang R, Chavez I, Taute K M, Lukic B, Jeney S, Raizen M G and Florin E-L 2011 *Nature Phys.* **7** 576
- [19] Katayama Y, Burkacky O, Meyer M, Bräuchle C, Gratton E and Lamb D C 2009 *Chem. Phys. Chem.* **10** 2458
- [20] Han Y, Alsayed A M, Nobili M, Zhang J, Lubensky T C and Yodh A G 2006 *Science* **314** 626
- [21] Fakhri N, MacKintosh F C, Lounis B, Cagnet L and Pasquali M 2010 *Science* **330** 1804
- [22] Montroll E W and Weiss G H 1969 *J. Math. Phys.* **10** 753
- [23] Scher H and Montroll E W 1975 *Phys. Rev. B* **12** 2455
- [24] Sokolov I M, Heinsalu E, Hänggi P and Goychuk I 2009 *Europhys. Lett.* **86** 30009
- [25] Barkai E, Metzler R and Klafter J 2000 *Phys. Rev. E* **61** 132
- [26] Bel G and Barkai E 2005 *Phys. Rev. Lett.* **94** 240602
- [27] Metzler R, Barkai E and Klafter J 1999 *Phys. Rev. Lett.* **82** 3563
- [28] Jeon J-H and Metzler R 2010 *Phys. Rev. E* **81** 021103
- [29] Cherstvy A G, Chechkin A V and Metzler R 2013 *New J. Phys.* **15** 083039
- Cherstvy A G, Chechkin A V and Metzler R 2014 *Soft Matter* **10** 1591
- [30] Jeon J-H, Chechkin A V and Metzler R 2014 *Phys. Chem. Chem. Phys.* **16** 15811
- [31] Safdari H, Chechkin A V, Jafari G and Metzler R 2015 *Phys. Rev. E* **91** 042107
- [32] Cherstvy A G and Metzler R 2015 *J. Stat. Mech.* P05010
- [33] Bodrova A, Chechkin A V, Cherstvy A G and Metzler R 2015 *New J. Phys.* **17** 063038
- [34] Goychuk I 2012 *Adv. Chem. Phys.* **150** 187
- [35] Weiss M 2013 *Phys. Rev. E* **88** 010101(R)
- [36] Saxton M J 1994 *Biophys. J.* **66** 394
- [37] Sung B J and Yethiraj A 2006 *Phys. Rev. Lett.* **96** 228103
- [38] Höfling F, Franosch T and Frey E 2006 *Phys. Rev. Lett.* **96** 165901
- [39] Skinner T O E, Schnyder S K, Aarts D G A L, Horbach J and Dullens R P A 2013 *Phys. Rev. Lett.* **111** 128301
- [40] Schnyder S K, Spanner M, Höfling F, Franosch T and Horbach J 2015 *Soft Matter* **11** 701
- [41] Mardoukhi Y, Jeon J-H and Metzler R 2015 *Phys. Chem. Chem. Phys.* at press (doi:10.1039/C5CP03548A)
- [42] Zimmerman S B and Minton A P 1993 *Ann. Rev. Biophys. Biomol. Struct.* **22** 27
- [43] Zhou H X, Rivas G and Minton A P 2008 *Ann. Rev. Biophys.* **37** 375
- [44] Denton A R 2014 *Intl. Rev. Cell & Molec. Biol.* **307** 27
- [45] Weiss M 2014 *Rev. Cell & Molec. Biol.* **307** 383
- [46] McGuffee A R and Elcock A H 2010 *PLoS Comp. Biol.* **6** e1000694
- [47] Spitzer J and Poolman B 2009 *Microbiol. Mol. Biol. Rev.* **73** 371
- [48] Müller K W, Bruinsma R F, Lieleg O, Bausch A R, Wall W A and Levine A J 2014 *Phys. Rev. Lett.* **112** 238102
- [49] Kühn T, Ihalainen T O, Hyväluoma J, Dross N, Willman S F, Langowski J, Vihinen-Ranta M and Timonen J 2011 *PLoS One* **6** e22962
- [50] English B P, Haurlyuk V, Sanamrad A, Tankov S, Dekker N H and Elf J 2011 *Proc. Natl. Acad. Sci. USA* **108** E365
- [51] Parry B R, Surovtsev I V, Cabeen M T, O'Hern C S, Dufresne E R and Jacobs-Wagner C 2014 *Cell* **156** 183
- [52] Szymanski J and Weiss M 2009 *Phys. Rev. Lett.* **103** 038102
- [53] Jeon J-H, Lejinse N, Oddershede L B and Metzler R 2013 *New J. Phys.* **15** 045011
- [54] Manzo C, Torreno-Pina J A, Massignan P, Lapeyre G J Jr, Lewenstein M and Parajo M F G 2015 *Phys. Rev. X* **5** 011021
- [55] Weigel A V, Simon B, Tamkun M M and Krapf D 2011 *Proc. Natl. Acad. Sci. USA* **108** 6438
- [56] Tabei S M A, Burov S, Kim H Y, Kuznetsov A, Huynh T, Jurellier J, Philipson L H, Dinner A R and Scherer N F 2013 *Proc. Natl. Acad. Sci. USA* **110** 4911
- [57] Jeon J-H, Tejedor V, Burov S, Barkai E, Selhuber-Unkel C, Berg-Sorensen K, Oddershede L and Metzler R 2011 *Phys. Rev. Lett.* **106** 048103
- [58] Ernst D, Köhler J and Weiss M 2014 *Phys. Chem. Chem. Phys.* **16** 7686
- [59] Saxton M J 2014 *J. Phys. Chem. B* **118** 12805
- [60] Saxton M J 2012 *Biophys. J.* **103** 2411
- [61] Berry H and Chate H 2014 *Phys. Rev. E* **89** 022708
- [62] Trovato F and Tozzini V 2014 *Biophys. J.* **107** 2579
- [63] Godec A, Bauer M and Metzler R 2014 *New J. Phys.* **16** 092002
- [64] Putzel G G, Tagliacucchi M and Szleifer I 2014 *Phys. Rev. Lett.* **113** 138302
- [65] Kim J, Backman V and Szleifer I 2011 *Phys. Rev. Lett.* **106** 168102
- [66] Shin J, Cherstvy A G and Metzler R 2014 *New J. Phys.* **16** 053047
- [67] Shin J, Cherstvy A G and Metzler R 2015 *Soft Matter* **11** 472
- [68] Shin J, Cherstvy A G and Metzler R 2015 *ACS Macro. Lett.* **4** 202
- [69] Kang H, Pincus P A, Hyeon C and Thirumalai D 2015 *Phys. Rev. Lett.* **114** 068303
- [70] Kang H, Toan N M, Hyeon C and Thirumalai D 2015 *J. Amer. Chem. Soc.* **137** 10970
- [71] Chapman D, Gorczyca S and Robertson-Anderson R M 2015 *Biophys. J.* **108** 1220
- [72] Ghosh S, Cherstvy A G and Metzler R 2015 *Phys. Chem. Chem. Phys.* **17** 1847

- [73] Ghosh S, Cherstvy A G, Grebenkov D S and Metzler R arXiv:1508.02029
- [74] Vasanthi R, Ravichandran S and Bagchi B 2001 *J. Chem. Phys.* **115** 10022
- [75] Cieřla M, Dybiec B, Gudowska-Nowak E and Sokolov I M 2014 *J. Chem. Phys.* **140** 044706
- [76] Hunter G L and Weeks E R 2012 *Rep. Prog. Phys.* **75** 066501
- [77] Sciortino F and Tartaglia P 2005 *Adv. Phys.* **54** 471
- [78] Berthier L and Witten T A 2009 *Phys. Rev. E* **80** 021502
- [79] Berthier L and Biroli G 2011 *Rev. Mod. Phys.* **83** 587
- [80] Debenedetti P G and Stillinger F H 2001 *Nature* **410** 259
- [81] Perera D N and Harrowell P 1999 *Phys. Rev. E* **59** 5721
- [82] Bayer M, Brader J M, Ebert F, Fuchs M, Lange E, Maret G, Schilling R, Sperl M and Wittmer J P 2007 *Phys. Rev. E* **76** 011508
- [83] Weysser F and Hajnal D 2011 *Phys. Rev. E* **83** 041503
- [84] Mazoyer S, Ebert F, Maret G and Keim P 2009 *Europhys. Lett.* **88** 66004
- [85] Santen L and Krauth W 2000 *Nature* **405** 550
- [86] Reis P M, Ingale R A and Shattuck M D 2007 *Phys. Rev. Lett.* **98** 188301
- [87] Lee C C, MacKay J A, Frechet J M J and Szoka F C 2005 *Nature Biotech.* **23** 1517
- [88] Frauenrath H 2005 *Progr. Polym. Sci.* **30** 325
- [89] Dobrynin A V 2008 *Curr. Opin. Coll. & Interf. Sci.* **13** 376
- [90] Winkler R G and Cherstvy A G 2014 *Adv. Polym. Sci.* **255** 1
- [91] Borisov O V, Polotsky A A, Rud O V, Zhulina E B, Leermakker F A M and Birshtein T M 2014 *Soft Matter* **10** 2093
- [92] Vlassopoulos D, Fytas G, Pakula T and Roovers J 2001 *J. Phys.: Condens. Matter* **13** R855
- [93] Blavatska V and Metzler R 2015 *J. Phys. A: Math. Theor.* **48** 135001
- [94] Yethiraj A and Hall C K 1991 *Macromol.* **24** 709
- [95] Saxton M J 2007 *Biophys. J.* **92** 1178  
Saxton M J 2000 *Biophys. J.* **81** 2226
- [96] Yamamoto E, Akimoto T, Yasui M and Yasuoka K 2014 *Sci. Rep.* **4** 4720
- [97] Jeon J-H, Monne H M, Javanainen M and Metzler R 2012 *Phys. Rev. Lett.* **109** 188103
- [98] Javanainen M, Hammaren H, Monticelli L, Jeon J-H, Miettinen M S, Martinez-Seara H, Metzler R and Vattulainen I 2013 *Faraday Discuss.* **161** 397
- [99] Ehrig J, Petrov E P and Schuille P 2011 *New J. Phys.* **13** 045019
- [100] Ehrig J, Petrov E P and Schuille P 2011 *Biophys. J.* **100** 80
- [101] Dlugosz M and Antosiewicz J M 2014 *J. Chem. Theor. Comput.* **10** 481
- [102] Balbo J, Merghetti P, Herten D P and Wade R C 2013 *Biophys. J.* **104** 1576
- [103] Singh S P, Huang C C, Westphal E, Gompper G and Winkler R G 2014 *J. Chem. Phys.* **141** 084901
- [104] Echeverria C and Kapral R 2012 *Phys. Chem. Chem. Phys.* **14** 6755
- [105] Allen M P and Tildesley D J 1987 *Computer Simulations of Liquids* (Oxford: Clarendon)
- [106] Bickmore W A and Sutherland H G E 2002 *EMBO J.* **21** 1248
- [107] Bouchaud J-P 1992 *J. Phys. I* **2** 1705
- [108] Bel G and Barkai E 2005 *Phys. Rev. Lett.* **94** 240602
- [109] Rebenshtok A and Barkai E 2007 *Phys. Rev. Lett.* **99** 210601
- [110] Deng W and Barkai E 2009 *Phys. Rev. E* **79** 011112
- [111] Lubelski A, Sokolov I M and Klafter J 2008 *Phys. Rev. Lett.* **100** 250602
- [112] He Y, Burov S, Metzler R and Barkai E 2008 *Phys. Rev. Lett.* **101** 058101
- [113] Jeon J-H, Barkai E and Metzler R 2013 *J. Chem. Phys.* **139** 121916
- [114] Tejedor V and Metzler R 2010 *J. Phys. A* **43** 082002
- [115] Magdziarz M, Metzler R, Szczotka W and Zebrowski P 2012 *Phys. Rev. E* **85** 051103
- [116] Massignan P, Manzo C, Torreno-Pina J A, Garcia-Parako M F, Lewenstein M and Lapeyre G L Jr. 2014 *Phys. Rev. Lett.* **112** 150603
- [117] Godec A, Chechkin A V, Barkai E, Kantz H and Metzler R 2014 *J. Phys. A: Math. Theor.* **47** 492002
- [118] Metzler R, Sanders L P, Lomholt M A, Lizana L, Fogelmark K and Ambjörnsson T 2014 *Eur. Phys. J. Special Topics* **223** 3287
- [119] Sanders L P, Lomholt M A, Lizana L, Fogelmark K, Metzler R and Ambjörnsson T 2014 *New J. Phys.* **16** 113050
- [120] Schulz J H P, Barkai E and Metzler R 2013 *Phys. Rev. Lett.* **110** 020602  
Schulz J H P, Barkai E and Metzler R 2014 *Phys. Rev. X* **4** 011028
- [121] Cherstvy A, Chechkin A V and Metzler R 2014 *J. Phys. A* **47** 485002
- [122] Pham K, Puertas A, Bergholtz J, Egelhaaf S, Moussaïd A, Pusey P, Schofield A, Cates M, Fuchs M and Poon W 2002 *Science* **296** 104
- [123] Lee S E and Chakraborty A K 2002 *J. Chem. Phys.* **117** 10869
- [124] Berezhkovskii A M, Dagdug L and Bezrukov S M 2014 *Biophys. J.* **106** L09
- [125] Burov S and Barkai E 2008 *Phys. Rev. Lett.* **100** 070601  
Burov S and Barkai E 2008 *Phys. Rev. E* **78** 031112
- [126] Kursawe J, Schulz J H P and Metzler R 2013 *Phys. Rev. E* **88** 062124
- [127] Tokuyama M and Oppenheim I 1994 *Phys. Rev. E* **50** R16
- [128] Tokuyama M and Oppenheim I 1995 *Physica A* **216** 85
- [129] van Blaaderen A, Peetermans J, Maret G and Dhont J K G 1992 *J. Chem. Phys.* **96** 4591
- [130] Phillips R J 2000 *Biophys. J.* **79** 3350
- [131] Franosch T, Fuchs M, Götze W, Mayr M R and Singh A P 1997 *Phys. Rev. E* **55** 7153
- [132] Kondrat S, Zimmermann O, Wiechert W and von Lieres E 2015 *Phys. Biol.* **12** 046003
- [133] Chakraborty A, Konya A, Wang F, Selinger J V, Sun K and Wei Q H 2014 *Langmuir* **30** 13844  
Chakraborty A, Konya A, Wang F, Selinger J V, Sun K and Wei Q H 2013 *Phys. Rev. Lett.* **111** 160603